ACS OMEGA

Open Access

http://pubs.acs.org/journal/acsodf

Article

OEEF-Driven Intramolecular Self-Redox of Superalkali $Rb_3BeB_6Be'Rb'_3$: A High-Performance Candidate for NLO Molecular Switch

Jia-Mei Zeng, Qin Liu, Jing-Yi Zhao, Rui Deng, Yin-Feng Wang,* Jiangen Huang, and Zhi-Ru Li*

Cite This: *ACS Omega* 2023, 8, 30612−30620

Read Online

ACCESS | Metrics & More | Article Recommendations | Supporting Information

ABSTRACT: To provide a novel intramolecular self-redox switch, a boron-based sandwich-like complex $Rb_3BeB_6Be'Rb'_3$ is achieved by using theoretical computations. An applicable oriented external electric field (OEEF) can result in the occurrence of intramolecular self-redox (IMSR) with a long-range electron transfer from tetrahedral $Be'Rb'_3$ to Rb_3Be and subsequently $[Rb_3Be]^{3+}[B_6]^{6-}[Be'Rb'_3]^{3+}$ (D_{3d}) changes to $[Rb_3Be]^{2+}[B_6]^{6-}[Be'Rb'_3]^{4+}$ (C_{3v}), accompanying high-performance NLO switchable effect for both static and dynamic first hyperpolarizability (β_0). $[Rb_3Be]^{3+}[B_6]^{6-}[Be'Rb'_3]^{3+}$ (off-form) owns zero of dipole moment (μ_0) and β_0, while $[Rb_3Be]^{2+}[B_6]^{6-}[Be'Rb'_3]^{4+}$ (on-form) exhibits a μ_0 of 3.36 D and a β_0^e of 2.18 × 10^5 au. The different dynamic first hyperpolarizabilities between $[Rb_3Be]^{3+}[B_6]^{6-}[Be'Rb'_3]^{3+}$ and $[Rb_3Be]^{2+}[B_6]^{6-}[Be'Rb'_3]^{4+}$ are also significant. This indicates that $Rb_3BeB_6Be'Rb'_3$ is a potential candidate for an IMSR NLO switch.

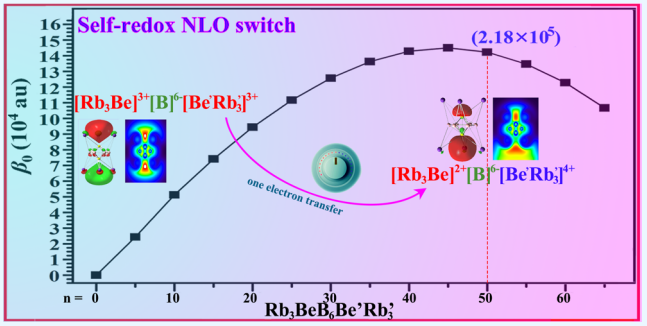

INTRODUCTION

The study of the effect of oriented external electric field (OEEF) on the chemical reaction and molecular material has been a fast-growing activity research field.[1−3] For chemical reactions, it is reported that OEEF can be responsible for the electrostatic catalysis in enzymes,[4−6] controlling the reactivity and selectivity of the famous Diels−Alder, proton transfer reactions, etc.[7−9] Even the OEEF has been suggested to be a promising candidate for use in future smart- and green-synthetic chemistry.[1,10] Under the influence of the OEEFs, unusual structures, special chemical bonds, and novel physical and chemical properties of the molecules can be found. Earlier, Li et al.[11,12] have reported that the OEEF can drive the hydrogen bond in $H_3N\cdots HCl$ to change into an ionic bond. In the nano field, the OEEF can change the energy band structure of nanotube and graphene to regulate their properties.[2]

The design and achievement of molecular switching materials are undoubtedly one of the most important goals in molecular electronics. To date, a massive number of nonlinear optical (NLO) molecular switches[13−29] have been obtained on both theoretical and experimental aspects because it is of paramount importance to the signal processing, data storage, sensing, and molecular devices.[13] As we have seen, the switching processes of the reported OEEF-driven charging molecular switches[20−27] and redox NLO switches[27−29] mainly relate to the change of the electron number while their three-dimensional molecular frameworks usually change little. So, these redox/charging switches may be a better choice due to the requirement of a terminal device or assembly of molecules. For the charging NLO molecular switches, it was reported that an applicable OEEF can lead to long-range excess electron transfers (LEET) in M^--$LCa^{2+}L$-M^- (M = Li or Na, L = $F_6C_6H_6$) and $e^-+Ca^{2+}(Ni@Pb_{12})^{2-}Ca^{2+}+e^-$, and consequently, both exhibit large static first hyperpolarizabilities (β_0).[20,21] For the redox NLO molecular switch, based on the pyridine helical complex, Xu et al.[28] have explored the effect of two-electron-redox process of Li_2-doped single-strand pyridine helical (Li_2@helical) on the NLO responses. In the single molecular level, we have presented that superalkali Li_3N_3Mg can be a good candidate for an intramolecular self-redox (IMSR) NLO switch due to the change from $Li_3^{2+}N_3Mg^+$ to $Li_3^+N_3Mg^{2+}$.[27]

In 2020, Wang et al. have presented that a unique boron-based sandwich cluster $Rb_6Be_2B_6$ with the D_{3d} point group is viable in the ionic complex of $[Rb_3Be]^{3+}[B_6]^{6-}[BeRb_3]^{3+}$.[30] To differentiate the two tetrahedral $BeRb_3$ ligands, $Rb_6Be_2B_6$ is named $Rb_3BeB_6Be'Rb'_3$ or $[Rb_3Be]^{3+}[B_6]^{6-}[Be'Rb'_3]^{3+}$ in this study. Then, like the effect of OEEF on M^--$LCa^{2+}L$-M^- (M =

Received: June 15, 2023
Accepted: July 24, 2023
Published: August 8, 2023

Li or Na, $L = F_6C_6H_6$) and $e^- + Ca^{2+}(Ni@Pb_{12})^{2-}Ca^{2+} + e^-$,[20,21] can an appropriate OEEF also result in the breaking of the symmetric electron clouds of D_{3d} $[Rb_3Be]^{3+}[B_6]^{6-}[Be'Rb'_3]^{3+}$ and lead to a LEET to form an IMSR switch? Subsequently, what is the value of β_0 of it? In that case, the boron-based sandwich cluster $Rb_6Be_2B_6$ may be a high-performance candidate for the IMSR NLO molecular switch. We hope that this work can provide a meaningful guidance and theoretical support for the regulation and control of electric field on the chemical reaction and molecular materials.

COMPUTATIONAL DETAILS

In this work, all quantum chemistry calculations, including geometrical optimization, frequency calculation, were done by using Gaussian16 (version A.03) program.[31] For the field-free $Rb_3BeB_6Be'Rb'_3$, it is reported[30] that the global minimum (GM) structure adopts a D_{3d} symmetry, and its structure was optimized at the PBE0[32]/def2-qzvp[33] level, which has been suggested to be reliable for the study of boron-based clusters.[34−37] Then, based on this structure, the optimized geometries for each stationary point of $Rb_3BeB_6Be'Rb'_3$ with different OEEFs were also calculated at the PBE0/def2-qzvp level. The natural population analysis (NPA)[38] was calculated at the MP2, PBE0, and CASSCF(2,2) methods with def2-qzvp basis set. The solvent effects are included using the polarizable continuum model (PCM), and the solvents of THF and cyclohexane (C_6H_{12}) are used. The quantum theory of atoms in molecules (QTAIM) analysis,[39] electron localization function (ELF) diagrams, and localized-orbital locator (LOL) plots as well as the transition orbital maps were obtained with Multiwfn program package (version 3.8).[40]

The VIE was determined as

$$\mathrm{VIE} = E[Rb_3BeB_6Be'Rb'_3]^+ - E[Rb_3BeB_6Be'Rb'_3] \quad (1)$$

where $E[Rb_3BeB_6Be'Rb'_3]^+$ and $E[Rb_3BeB_6Be'Rb'_3]$ are the energies of the $[Rb_3BeB_6Be'Rb'_3]^+$ cation and $[Rb_3BeB_6Be'Rb'_3]$. Both were calculated with the same geometry as that of neutral $Rb_3BeB_6Be'Rb'_3$.

In general, for a nonspherically symmetric molecule in an OEEF, if the orientation dependence of OEEF effect is ignored, the magnitude order of the electron tunneling ionization rate (ω) can be roughly obtained from the following formula:[41,42]

$$\omega = 4\frac{\omega_0}{|F|}(2\mathrm{VIE})^{5/2}\exp\left[-\frac{2(2\mathrm{VIE})^{3/2}}{3|F|}\right] \quad (2)$$

where both F and VIE are measured in atomic units and $\omega_0 = 4 \times 10^{16}$ s^{-1}.

It is known that, if the finite field (FF) approach is used to evaluate the β_0 value, there may occur a contamination risk from higher-order hyperpolarizabilities[43,44]

$$\beta(F) = 2\frac{\mu(2F) - \mu(F)}{F} = \frac{2\boldsymbol{E}_A(F) - \boldsymbol{E}_A(2F)}{F^3} = \beta + \frac{\delta F^2}{4} + O(F^4) \quad (3)$$

However, it can be eliminated by using the Richardson extrapolation procedure.[42,43] In our previous study, it has been shown that the above contamination can be ignored for several excess electron compounds.[24−26] Then, a field amplitude of 10×10^{-4} au was used for the FF method. The optimized structures of $Rb_6Be_2B_6$ without the presence of F_z were considered.

For the β_0 value of electride Li@pyrrole, it has been suggested[45] that the MP2 value is close to the expensive higher-order QCISD one. Also, for some similar electride systems,[26,27] the MP2 method is reliable to investigate the β_0 values. M06-2X not only exhibits positive behavior for calculating electronic structures, but it is also widely utilized to calculate β_0 values.[21,22,46] Therefore, the β_0^e values of $Rb_3BeB_6Be'Rb'_3$ were obtained at both M06-2X/def2-qzvp and MP2/def2-qzvp levels. The electronic spectra were obtained with the time-dependent TD-PBE0/def2-qzvp level. To find which excitation path(s) makes the main contribution to the total β_0^e, 250 excited states are considered.

The β_0^e is noted as

$$\beta_0^e = (\beta_x^2 + \beta_y^2 + \beta_z^2)^{1/2} \quad (4)$$

The Bishop−Hasan−Kirtman (BHK) approach[47] is applied to calculate the vibrational contribution to static first hyperpolarizability (β_{zzz}^{nr}). This method is a numerical approach. The β_{zzz}^{nr} is written by the following equations

$$\beta_{zzz}^{tot} = \beta_{zzz}^{e} + \beta_{zzz}^{nr} \quad (5)$$

$$\beta_{zzz,tot} = \frac{[\Delta\mu_{i,z}(R_F, F_{z,i})] + 2\Delta\mu_z(R_{Fw}, Fw_z) + [\Delta\mu_{ii,z}(R_F, F_{z,ii})]}{\Delta F^2} \quad (6)$$

$$\Delta\mu_z(R_F, F_z) = \mu_z(R_F, F_z) - \mu_z(R_{Fw}, Fw_z) \quad (7)$$

where β_{zzz}^{tot} represents the total static first hyperpolarizability, the electronic and vibrational contribution to β_{zzz}^{tot} were, respectively, written as β_{zzz}^{e} and β_{zzz}^{nr}; $\Delta\mu_z(R_F, F_z)$ is the difference of dipole moments between dipole moment of test ($\mu_z(R_F, F_z)$) and that of work OEEF ($\mu_z(R_{Fw}, Fw)$); and R_F represents the equilibrium geometry in the presence of an OEEF.

The frequency-dependent NLO properties ($\beta(-2\omega,\omega,\omega)$) of $Rb_3BeB_6Be'Rb'_3$ were calculated at the PBE0/def2-qzvp level. Imitating to the reported multiplicative scheme,[13] the $\beta(-2\omega,\omega,\omega)$ values at MP2 method were estimated by

$$\beta_{MP2}(-2\omega; \omega, \omega) \approx \beta_{MP2}(0; 0, 0) \times \beta_{TD-M06-2X}(-2\omega; \omega, \omega) / \beta_{CP-M06-2X}(0; 0, 0) \quad (8)$$

The molecular structures and molecular orbitals as well as the electronic absorption spectra were plotted with GaussView program.[48]

RESULTS AND DISCUSSION

Self-Redox from $[Rb_3Be]^{3+}[B_6]^{6-}[Be'Rb'_3]^{3+}$ to $[Rb_3Be]^{2+}[B_6]^{6-}[Be'Rb'_3]^{4+}$. The optimized structure with all real frequencies of D_{3d} $Rb_3BeB_6Be'Rb'_3$ is shown in Figure 1. According to the NPA charge analysis, the valences of both tetrahedral $BeRb_3$ ligands are +3. Then, the salt-like structure has been suggested to be $[Rb_3Be]^{3+}[B_6]^{6-}[Be'Rb'_3]^{3+}$.[30] Our calculations can acknowledge it by using the data from NPA charges at MP2, PBE0, and CASSCF(2,2) methods with the def2-qzvp basis set (see Table 1). The values in Table 1 indicate that the NPA charges calculated at MP2/def2-qzvp,

https://doi.org/10.1021/acsomega.3c04248
ACS Omega 2023, 8, 30612−30620

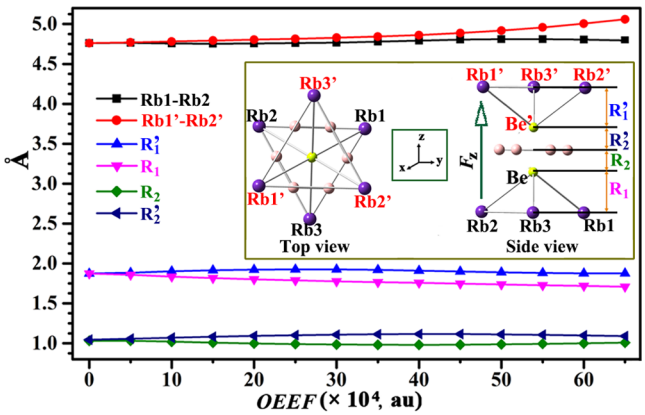

Figure 1. Evolution of bond lengths of $Rb_3BeB_6Be'Rb'_3$ with the increasing external electric field strength (F_z).

Table 1. NPA Charges of Q_{Rb_3Be}, Q_{B_6}, and $Q_{Be'Rb'_3}$ in $Rb_3BeB_6Be'Rb'_3$ with Respect to OEEF (F_z) at Different Methods

	F_z ($\times 10^{-4}$ au)			
	0	50	55	65
MP2/def2-qzvp				
Q_{Rb_3Be}	2.756	2.058	1.932	1.792
Q_{B_6}	−5.513	−5.546	−5.559	−5.560
$Q_{Be'Rb'_3}$	2.756	3.488	3.626	3.768
PBE0/def2-qzvp				
Q_{Rb_3Be}	2.820	2.364	2.286	2.093
Q_{B_6}	−5.640	−5.651	−5.660	−5.663
$Q_{Be'Rb'_3}$	2.820	3.287	3.374	3.570
CASSCF(2,2)/def2-qzvp				
Q_{Rb_3Be}	2.828	2.474	1.838	1.863
Q_{B_6}	−5.657	−5.674	−5.673	−5.691
$Q_{Be'Rb'_3}$	2.828	3.202	3.348	3.637

PBE0/def2-qzvp, and CASSCF(2,2)/def2-qzvp levels are 2.756, 2.820, and 2.828 lel, respectively, for both $[Rb_3Be]$ and $[Be'Rb'_3]$.

In the present work, considering a larger OEEF ($F_z \geq 65 \times 10^{-4}$ au) will destroy the geometrical structure of $Rb_3BeB_6Be'Rb'_3$, $F_z = 65 \times 10^{-4}$ au (1 au = 51.422 V/Å) is used as a critical value (F_c). Then, the OEEF along with the dipole moment direction (F_z, see Figure 1) for $Rb_3BeB_6Be'Rb'_3$ is in the range of $0-65 \times 10^{-4}$ au. To estimate the effect of OEEF on the geometrical structure, some important geometrical parameters (Rb−Rb length, R_1, R_2, R_1', and R_2') of $Rb_3BeB_6Be'Rb'_3$ were collected and are listed in Table S1. From Figure 1 and Table S1, it can be found that, as the magnitude of F_z increases, the Rb′−Rb′ bond length and the distance between Be' atom and the center of Rb'_3 ring (R1′) in top tetrahedral $Be'Rb'_3$ slightly increase, while both Rb−Rb bond length and R1 in bottom tetrahedral Rb_3Be almost do not change. As a result, D_{3d} $Rb_3BeB_6Be'Rb'_3$ with two identical tetrahedral ligands (Rb_3Be = $Be'Rb'_3$) changes into C_{3v} $Rb_3BeB_6Be'Rb'_3$ with one slightly larger ($Be'Rb'_3$) and one smaller tetrahedral ligand (Rb_3Be). However, there is only small (<0.3 Å) increases of Rb′−Rb′ bond length in $Be'Rb'_3$ in the presence of $F_z = 65 \times 10^{-4}$ au as compared to Rb_3Be for field-free $Rb_3BeB_6Be'Rb'_3$. This behavior may be beneficial for the molecular assembly of $Rb_3BeB_6Be'Rb'_3$ in the terminal devices.

The larger the size of the tetrahedral structure has, the larger the NPA charge or the fewer the number of electrons it owns. The results in Figure 2a and Table 1 as well as Table S2 show that, at the MP2/def2-qzvp level, the NPA charge of the top tetrahedral $Be'Rb'_3$ increases but that of bottom tetrahedral Rb_3Be decreases along with an increase in the magnitude of F_z. Meanwhile, the NPA charge of the B_6 ring does not change evidently. As $F_z = 50 \times 10^{-4}$ au, the NPA charges of $Be'Rb'_3$ and Rb_3Be are 3.488 and 2.058 lel, respectively, and the NPA charges in each case are 3.626 and 1.932 lel, respectively, as $F_z = 55 \times 10^{-4}$ au. For an even larger F_z of 65×10^{-4} au, the NPA charges are 3.768 and 1.792 lel, respectively, for $Be'Rb'_3$ and Rb_3Be. These show that the valences of $Be'Rb'_3$ and Rb_3Be in $Rb_3BeB_6Be'Rb'_3$ in the presence of $F_z \geq 50 \times 10^{-4}$ au are +4 and +2, respectively. Similar NPA behaviors can be confirmed using both PBE0/def2-qzvp and CASSCF(2,2)/def2-qzvp levels (see Table 1).

Considering the solvent effect, we have calculated the NPA charges of $Rb_3BeB_6Be'Rb'_3$ with solvents of THF and cyclohexane (C_6H_{12}) in the presence of $F_z = 50 \times 10^{-4}$ au. From Table 2, at the PBE0/def2-qzvp level, the NPA charges of $Be'Rb'_3$ and Rb_3Be are, respectively, 3.836 and 1.854 lel for the solvent of THF and are 3.507 and 2.181 lel for the solvent of C6H12. At the MP2/def2-qzvp level, the NPA charges of $Be'Rb'_3$ and Rb_3Be are, respectively, 4.455 and 1.205 lel for the solvent of THF and are 3.390 and 2.305 lel for the solvent of C_6H_{12}. These results show that the influence of a solvent on the redox reaction under the OEEF is not very large. In both solvents, the valences of $Be'Rb'_3$ and Rb_3Be in $Rb_3BeB_6Be'Rb'_3$ in the presence of $F_z = 50 \times 10^{-4}$ au are still +4 and +2, respectively.

The electron clouds of frontier molecular orbitals can provide support for this. The highest occupied molecular orbital (HOMO) and HOMO − 1 are also shown in Figure 2. For the HOMO, when the OEEF goes from 0 to 50 or 65×10^{-4} au, the shape of its orbital is changed from a symmetric dumbbell shape of two lobes to a larger and a smaller lobe. Similar behaviors can be seen in the ELF and LOL maps (see Figure 2b,c).

So, the salt-like structure of $Rb_3BeB_6Be'Rb'_3$ in the presence of $F_z \geq 50 \times 10^{-4}$ au is $[Rb_3Be]^{2+}[B_6]^{6-}[Be'Rb'_3]^{4+}$. These results indicate that applying a critical F_z of 50×10^{-4} au or even a larger one in the z-axis positive direction of the field-free $Rb_3BeB_6Be'Rb'_3$ can drive an electron to transfer from tetrahedral $Be'Rb'_3$ to Rb_3Be, and then, the IMSR occurs and $[Rb_3Be]^{3+}[B_6]^{6-}[Be'Rb'_3]^{3+}$ changes into $[Rb_3Be]^{2+}[B_6]^{6-}[Be'Rb'_3]^{4+}$.

Stabilities. Owing to the occurrence of OEEF(s), it deserves careful consideration of the stability of $[Rb_3Be]^{2+}[B_6]^{6-}[Be'Rb'_3]^{4+}$. The results on the stability are given in Figure 3 and Table S2. From Figure 3a and Table S2, one can found that the total energy monotonically decreases with increasing the intensity of OEEF in positive directions of z-axis (from $F_z = 0$ to 65×10^{-4} au). Therefore, the thermodynamic stability of $Rb_3BeB_6Be'Rb'_3$ is gaining strength along with an increase in the magnitude of F_z. $[Rb_3Be]^{2+}[B_6]^{6-}[Be'Rb'_3]^{4+}$ in the presence of $F_z \geq 50 \times 10^{-4}$ au possesses a higher thermodynamic stability than that of the $[Rb_3Be]^{3+}[B_6]^{6-}[Be'Rb'_3]^{3+}$ in the presence of $F_z < 50 \times 10^{-4}$ au. For a molecule, the electronic stability may be characterized by its VIE values. For the gap (ε_{gap}) between the

https://doi.org/10.1021/acsomega.3c04248
ACS Omega 2023, 8, 30612−30620

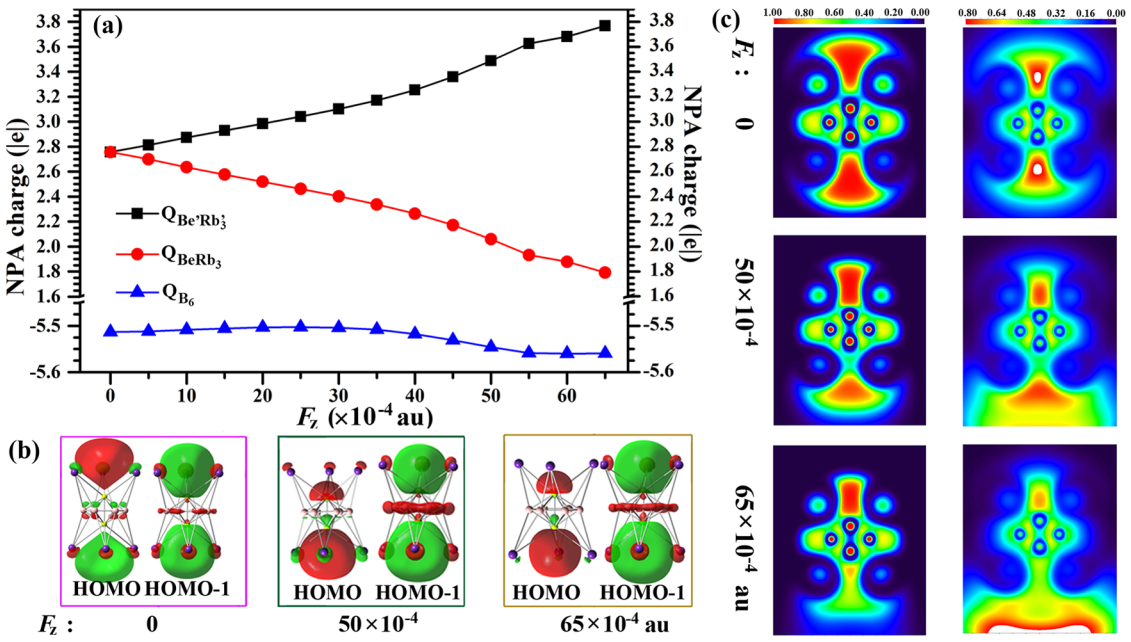

Figure 2. (a) Evolutions of NPA charges of $Rb_3BeB_6Be'Rb'_3$ with the increasing external electric field strength (F_z). (b) HOMOs at the isovalue of 0.02 au. (c) ELF maps and LOL maps of $Rb_3BeB_6Be'Rb'_3$ in the presence of different F_z.

Table 2. NPA Charges of Q_{Rb_3Be}, Q_{B_6}, and $Q_{Be'Rb'_3}$ in $Rb_3BeB_6Be'Rb'_3$ with Different Solvents at PBE0/def2-qzvp and MP2/def2-qzvp Levels in the Presence of F_z = 50 × 10^{-4} au

	PBE0		MP2	
	THF	C_6H_{12}	THF	C_6H_{12}
Q_{Rb_3Be}	1.854	2.181	1.205	2.305
Q_{B_6}	−5.690	−5.687	−5.660	−5.694
$Q_{Be'Rb'_3}$	3.836	3.507	4.455	3.390

HOMO and LUMO (lowest unoccupied molecular orbital), a large ε_{gap} value reflects high chemical stability. The results in Figure 3b,c and Table S2 show that the VIE value increases and the ε_{gap} value decreases along with an increase in the magnitude of F_z. So, the electronic stability ascends, and the molecular chemical stability descends along with an increase in the magnitude of F_z. As a result, $[Rb_3Be]^{2+}[B_6]^{6-}[Be'Rb'_3]^{4+}$ in the presence of $F_z \geq 50 \times 10^{-4}$ au owns a higher electronic stability but lower chemical stability than that of $[Rb_3Be]^{3+}[B_6]^{6-}[Be'Rb'_3]^{3+}$ in the presence of $F_z < 50 \times 10^{-4}$ au.

The ε_{gap} value of $[Rb_3Be]^{3+}[B_6]^{6-}[Be'Rb'_3]^{3+}$ in the presence of $F_z = 50 \times 10^{-4}$ au is 1.996 eV. It is smaller than that of the reported redox switch $Li_3^+N_3^{3-}Mg^{2+}$ in the presence of $F_z = 72 \times 10^{-4}$ and 86×10^{-4} au (2.327 and 2.314 eV).[27] However, it is much larger for $[Rb_3Be]^{3+}[B_6]^{6-}[Be'Rb'_3]^{3+}$ in the presence of $F_z = 50 \times 10^{-4}$ au than for the reported $K(1)^+\cdots$calix[4]pyrrole$\cdots K(2)^+\cdots 2e^-$ (1.315−1.719 eV)[49] and $e^-+Ca^{2+}(Ni@Pb_{12})^{2-}Ca^{2+}+2e^-$ (0.96−1.45 eV).[21] As a result, $[Rb_3Be]^{3+}[B_6]^{6-}[Be'Rb'_3]^{3+}$ in the presence of $F_z = 50 \times 10^{-4}$ au with larger ε_{gap} has larger chemical stability than the reported molecular switches of $e^-\cdots K(1)^+\cdots$calix[4]pyrrole$\cdots K(2)^+\cdots e^-$ and $e^-+M^{2+}(Ni@Pb_{12})^{2-}$ $M^{2+}+e^-$ (M = Be, Mg, and Ca). The VIEs of $Li_3^+N_3^{3-}Mg^{2+}$ in the presence of $F_z = 72 \times 10^{-4}$ and 86×10^{-4} au,[27] Li^--LCa^{2+}L-Li^-, Na^--LCa^{2+}L-Na^- (L = $F_6C_6H_6$),[20] and $e^-+Ca^{2+}(Ni@Pb_{12})^{2-}Ca^{2+}+2e^-$,[21] are 5.05, 5.05, 4.12, 4.04, and 4.48 eV. They are larger than (3.512 eV) that of $[Rb_3Be]^{3+}[B_6]^{6-}[Be'Rb'_3]^{3+}$ in the presence of $F_z = 50 \times 10^{-4}$ au.

In general, it is on a time scale of approximately 10−10^4 fs[50] for the occurrence of a chemical reaction. So, for a molecule under an OEEF, an order of magnitude threshold of around 10^{11} s^{-1} may be appropriate by taking the reciprocal of 10^{-4} fs^{-1} as the max acceptable average tunneling ionization rate (ω).[35] Given that, the ω values listed in Figure 3b and Table S2 indicate that except the structure in the presence of $F_z = 55 \times 10^{-4}$ au, all the ω values of other structures are smaller than 10^{11} s^{-1}. Therefore, except for the structure in the presence of $F_z = 55 \times 10^{-4}$ au, all the other structures of $[Rb_3Be]^{2+}[B_6]^{6-}[Be'Rb'_3]^{4+}$ may be stable.

Candidate for NLO Molecular Switches. Because the calculated β_0^e is sensitive to the OEEF,[43,44] the optimized structures of $[Rb_3Be]^{2+}[B_6]^{6-}[Be'Rb'_3]^{4+}$ with no consideration of the presence of F_z were used to calculate β_0^e. Considering the structural differentiation of $Rb_3BeB_6Be'Rb'_3$, their different structures are named $Rb_3BeB_6Be'Rb'_3(n)$, where n is the significant digit of magnitude of the initial F_z. Then, field-free $Rb_3BeB_6Be'Rb'_3(50)$ denotes the initial optimized structures of $[Rb_3Be]^{2+}[B_6]^{6-}[Be'Rb'_3]^{4+}$ in the presence of $F_z = 50 \times 10^{-4}$ au.

For β_0^e, it is noteworthy that Figure 4 and Table S3 show a pronounced discrepancy in the redox process at the M06-2X/def2-qzvp level. For the field-free $Rb_3BeB_6Be'Rb'_3$ ($[Rb_3Be]^{3+}[B_6]^{6-}[Be'Rb'_3]^{3+}$) with the D_{3d} point group, both μ_0 and β_0^e are zero. Then, $[Rb_3Be]^{3+}[B_6]^{6-}[Be'Rb'_3]^{3+}$ is the off-form of the IMSR NLO switch. The β_0^e or β_{zzz}^e value of $Rb_3BeB_6Be'Rb'_3(n)$ increases first and then decreases with an increase in the magnitude of n (n = 0−65). As n = 45, the β_0^e or β_{zzz}^e value reaches its maximum (1.45×10^5 au) at the M06-2X/def2-qzvp level. However, the neighboring $Rb_3BeB_6Be'Rb'_3(50)$, i.e., $[Rb_3Be]^{2+}[B_6]^{6-}[Be'Rb'_3]^{4+}$, has been used as the on-form of the redox NLO molecular switch considering the NPA charge of tetrahedral $Be'Rb'_3$ and Rb_3Be. The β_0^e values of $Rb_3BeB_6Be'Rb'_3(50)$ at the M06-2X/def2-

https://doi.org/10.1021/acsomega.3c04248
ACS Omega 2023, 8, 30612−30620

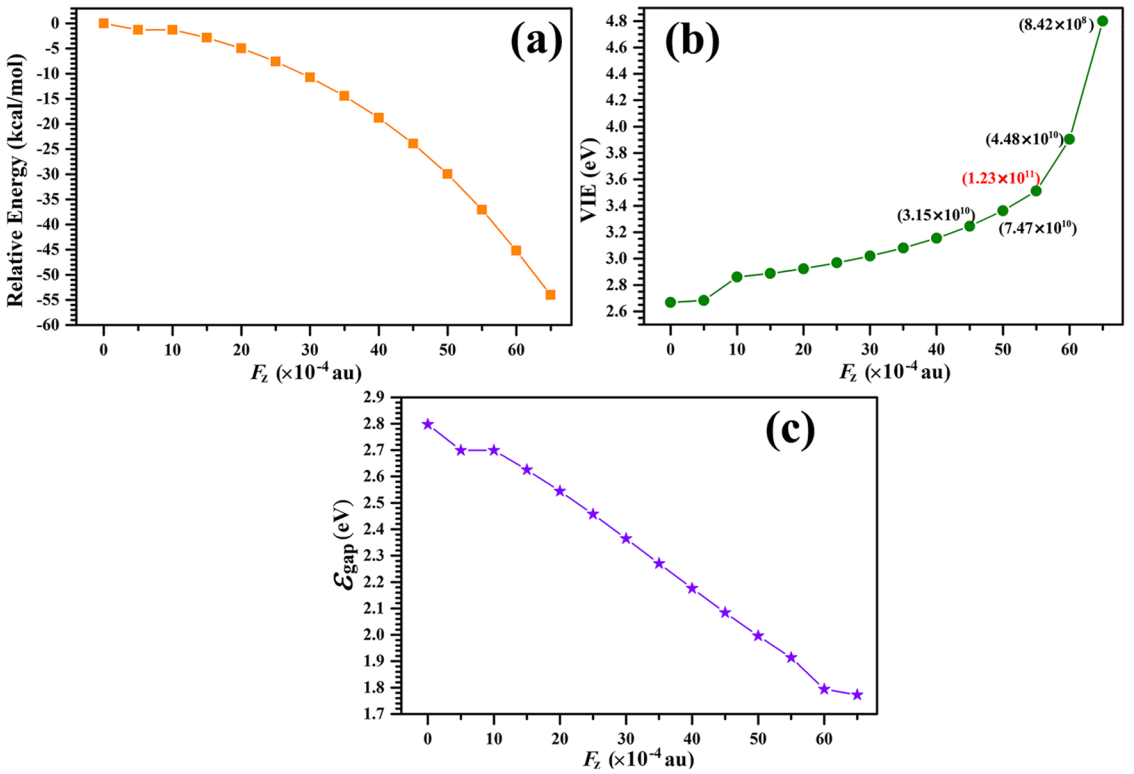

Figure 3. Evolutions of (a) relative energy (E_{rel}), (b) VIE, and (c) ε_{gap} of $Rb_3BeB_6Be'Rb'_3$ with increasing external electric field strength (F_z). The electron tunneling ionization rates (ω, s^{-1}) are within parentheses.

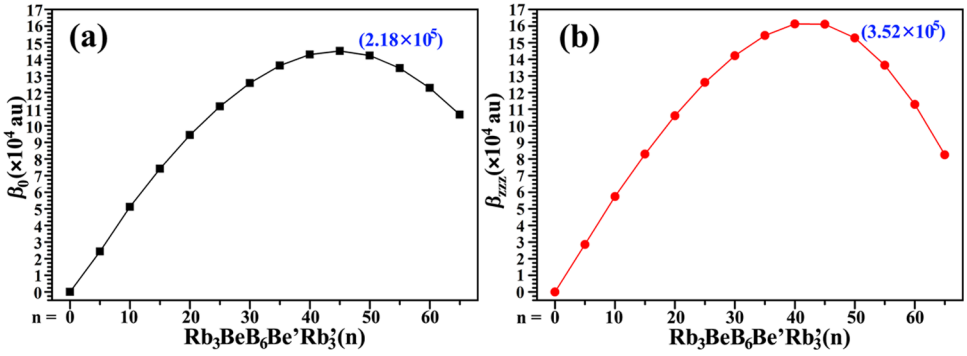

Figure 4. Evolutions of (a) β_0 and β_{zzz} values of $Rb_3BeB_6Be'Rb'_3$(n) with an increase in n (n = 0−65) at the M06-2X/def2-qzvp level. The MP2/def2-qzvp values are within parentheses.

qzvp and MP2/def2-qzvp levels are 1.42 × 10^5 and 2.18 × 10^5 au, respectively. Then, the μ_0 (3.36 D) and β_0^e (2.18 × 10^5 au) values of $[Rb_3Be]^{2+}[B_6]^{6-}[Be'Rb'_3]^{4+}$ ($Rb_3BeB_6Be'Rb'_3$(50)) at the MP2/def2-qzvp level have been used in the following discussion.

Owing to the D_{3d} symmetry, the dipole moment (μ_0) of $[Rb_3Be]^{3+}[B_6]^{6-}[Be'Rb'_3]^{3+}$ is zero. From Table 3, the μ_0 value of the C_{3v} $[Rb_3Be]^{2+}[B_6]^{6-}[Be'Rb'_3]^{4+}$ 3.36 D. Then, the dipole moment of $Rb_3BeB_6Be'Rb'_3$ exhibits a good performance NLO switching effect from $[Rb_3Be]^{3+}[B_6]^{6-}[Be'Rb'_3]^{3+}$ to $[Rb_3Be]^{3+}[B_6]^{6-}[Be'Rb'_3]^{4+}$.

The β_0^e (2.18 × 10^5 au) value of the on-form of $Rb_3BeB_6Be'Rb'_3$ ($[Rb_3Be]^{2+}[B_6]^{6-}[Be'Rb'_3]^{4+}$ = $Rb_3BeB_6Be'Rb'_3$(50)) is more than two times of that of the redox switch of $Li_3^+N_3^{3-}Mg^{2+}$ (1.01 × 10^5 au).[27] For the reported OEEF-induced NLO molecular switches, the β_0 values of on-forms of Lithium@cyclo[18]carbon,[19] Na^-−$LCa^{2+}L$−Na^- (L = $F_6C_6H_6$),[20] e^-+Ca^{2+}(Ni@Pb_{12})$^{2-}$$Ca^{2+}$+2$e^-$,[21] $Mg(NH_3)_6Na_2$,[22] Be_6Li_8,[23] Na-$(HCN)_3Na$,[24] K−$F_6C_6H_6$,[25] $Na(HF)_3Na$,[26] Li_2@helical,[28] $Ir(F_2PPY)_2ADC$,[29] and K(1)$^+$···calix[4]pyrrole···K(2)$^+$···2e^-,[49] are 2.25 × 10^3, 6.42 × 10^4, 2.2 × 10^6, 5.95 × 10^6, 5.4 × 10^4, 1.09 × 10^4, 4.67 × 10^5, 4.23 × 10^4, 7.73 × 10^6, 1.61 × 10^4, and 3.15 × 10^6 au,[48] respectively. Therefore, the β_0^e value of the on-form of $Rb_3BeB_6Be'Rb'_3$ is much larger than most of the reported OEEF-induced NLO molecular switches.

To study which excitation path is primarily contributed to β_0^e, for $Rb_3BeB_6Be'Rb'_3$, it can be estimated by using the following simplified sum-overstate (SOS) formula:[51]

$$\beta_0^e \propto (\Delta\mu \cdot f_0)/\Delta E^3 \quad (9)$$

For this formula, ΔE, f_0, and $\Delta\mu$ denote the electronic transition energy, oscillator strength, and the difference of transition dipole moment between the ground state and the crucial excited state, respectively. In this case, the most

https://doi.org/10.1021/acsomega.3c04248
ACS Omega 2023, 8, 30612−30620

Table 3. Dipole Moment (μ_0), β_0 and Its Values by Sum-Overstate Calculation (β_0^{SOS}), Difference of Dipole Moment between Ground State and Crucial Excited State ($\Delta\mu$), Oscillator Strength f_0, and Transition Energy (ΔE) of the Crucial Excited State for $[Rb_3Be]^{3+}[B_6]^{6-}[Be'Rb'_3]^{3+}$ (1) and $[Rb_3Be]^{2+}[B_6]^{6-}[Be'Rb'_3]^{4+}$ (2) at the PBE0/def2-qzvp Level

	μ_0 (D)	μ_z (D)	β_0^e (au)	β_{zzz}^e (au)	β_0^{SOS} (au)	$\Delta\mu_z$(au)	ΔE (eV)	f_0	λ (nm)
1	0.00	0.00	0.00	0.00	0.00	0.00	0.840	0.401	1477
						0.00	1.041	0.326	1191
						0.00	1.495	0.297	829
						0.00	1.518	0.679	817
						0.00	2.519	0.172	492
						0.00	3.075	0.146	403
						0.00	3.095	0.179	400
2	3.36	−3.36	2.18×10^5	3.52×10^5	2.90×10^5	2.43	0.783	0.340	1584
						−3.59	1.001	0.278	1238
						5.24	1.421	0.217	872
						2.56	1.469	0.704	844
						1.10	2.229	0.100	555
						1.18	3.09	0.192	400

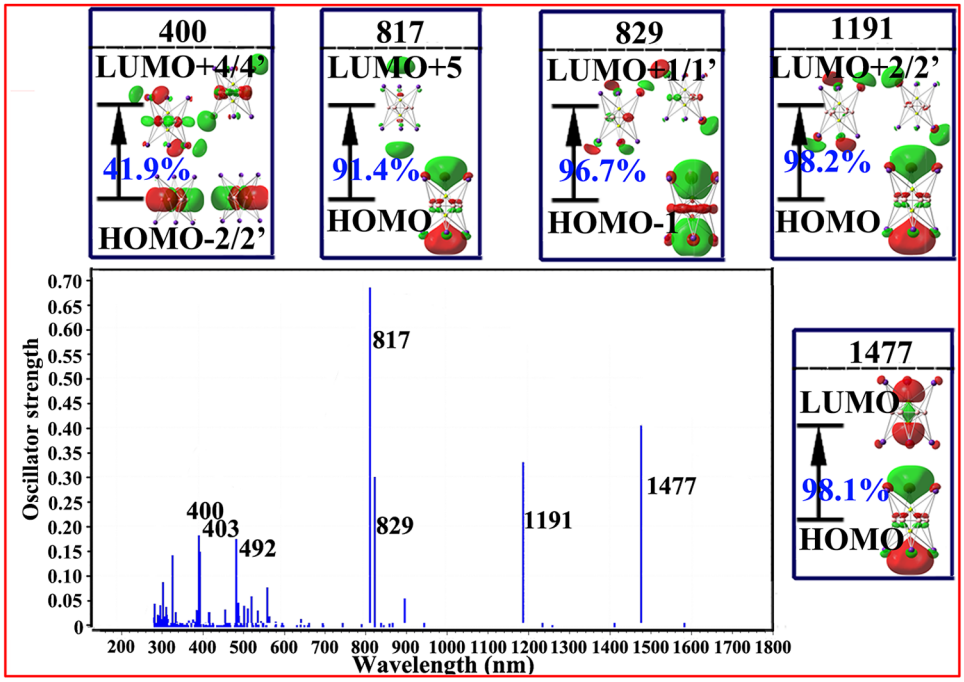

Figure 5. Electronic absorption spectrum of $[Rb_3Be]^{3+}[B_6]^{6-}[Be'Rb'_3]^{3+}$ (n = 0).

important factor is the excitation energy because β_0^e is proportional to the inversion of its cube.

The results in Figures 5 and 6 show that the intense absorption bands of both $[Rb_3Be]^{3+}[B_6]^{6-}[Be'Rb'_3]^{3+}$ ($Rb_3BeB_6Be'Rb'_3$(0), off-form) and $[Rb_3Be]^{2+}[B_6]^{6-}[Be'Rb'_3]^{4+}$ ($Rb_3BeB_6Be'Rb'_3$(50), on-form) come from many absorption peaks. Then, β_0^e involves a contribution of many excited states. Table 3 shows that the $\Delta\mu_z$ value is zero for $[Rb_3Be]^{3+}[B_6]^{6-}[Be'Rb'_3]^{3+}$ with the D_{3d} point group while that are not zero for $[Rb_3Be]^{2+}[B_6]^{6-}[Be'Rb'_3]^{4+}$ with C_{3v} one. Owing the zero of $\Delta\mu_z$, the β_0^{SOS} is zero for $[Rb_3Be]^{3+}[B_6]^{6-}[Be'Rb'_3]^{3+}$. In addition, from Figure 5, the wavelengths of these absorption peaks in the intense absorption band have an obvious blue shift from $[Rb_3Be]^{3+}[B_6]^{6-}[Be'Rb'_3]^{3+}$ to $[Rb_3Be]^{2+}[B_6]^{6-}[Be'Rb'_3]^{4+}$. For example, the maximum absorption peak (λ_{max}) in intense absorption band occurs at 817 nm for $[Rb_3Be]^{3+}[B_6]^{6-}[Be'Rb'_3]^{3+}$ while that broad shifts to 844 nm for $[Rb_3Be]^{2+}[B_6]^{6-}[Be'Rb'_3]^{4+}$. Considering these blue shifts, the ΔE value of each maximum absorption peak is smaller for $[Rb_3Be]^{2+}[B_6]^{6-}[Be'Rb'_3]^{4+}$ than that for $[Rb_3Be]^{3+}[B_6]^{6-}[Be'Rb'_3]^{3+}$.

By analyzing the vibrational first hyperpolarizability tensors (β_{zzz}^{nr}) of a series of excess electron compounds, Luis and co-workers have shown that the impact of vibrational hyperpolarizability is also vitally important.[46] Then, the β_{zzz}^{nr} values of both $[Rb_3Be]^{3+}[B_6]^{6-}[Be'Rb'_3]^{3+}$ and $[Rb_3Be]^{2+}[B_6]^{6-}[Be'Rb'_3]^{4+}$ were also calculated. Because the calculation of the harmonic Raman frequency is necessary to obtain the β_{zzz}^{nr} value, the β_{zzz}^{nr} values were obtained at the PBE0/def2-qzvp level. For the purpose of comparison, we also calculated β_{zzz}^e at the same level. From Table 4, it is shown that $[Rb_3Be]^{2+}[B_6]^{6-}[Be'Rb'_3]^{4+}$ holds a very small ratio η ($\beta_{zzz}^{nr}/\beta_{zzz}^e$), which suggests that the electronic contribution plays an important role and the vibrational contribution plays a secondary role only for the NLO response of

https://doi.org/10.1021/acsomega.3c04248
ACS Omega 2023, 8, 30612−30620

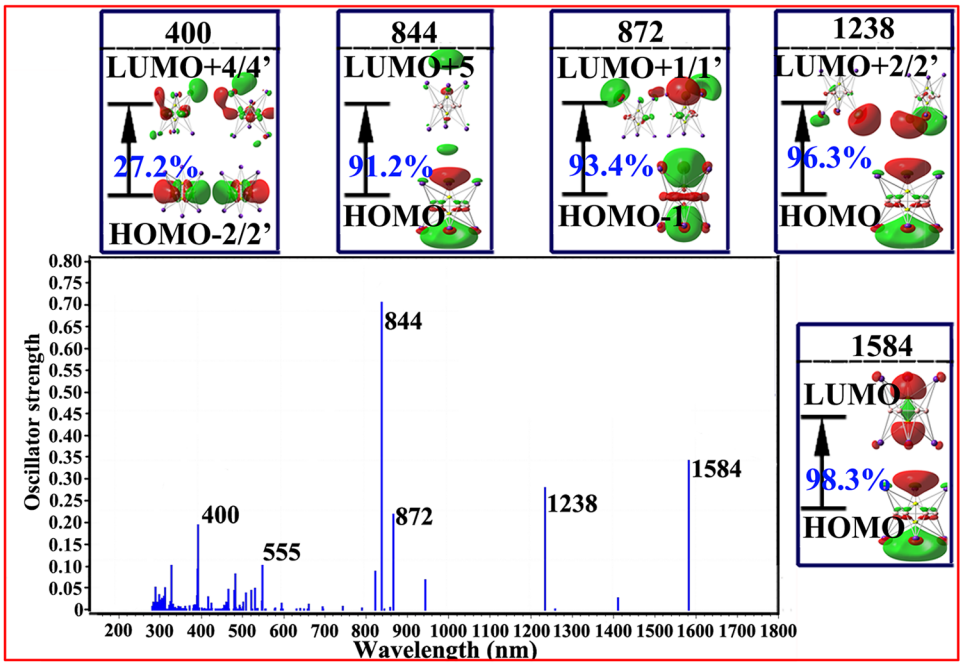

Figure 6. Electronic absorption spectrum of $[Rb_3Be]^{2+}[B_6]^{6-}[Be'Rb'_3]^{4+}$ (n = 50).

Table 4. Electronic First Hyperpolarizability Tensor β_{zzz}^{e}, Vibrational First Hyperpolarizability Tensor β_{zzz}^{nr}, and Ratio η of $\beta_{zzz}^{nr}/\beta_{zzz}^{e}$ for $[Rb_3Be]^{3+}[B_6]^{6-}[Be'Rb'_3]^{3+}$ and $[Rb_3Be]^{2+}[B_6]^{6-}[Be'Rb'_3]^{4+}$ at the PBE0/def2-qzvp Level

	$[Rb_3Be]^{3+}[B_6]^{6-}[Be'Rb'_3]^{3+}$	$[Rb_3Be]^{2+}[B_6]^{6-}[Be'Rb'_3]^{4+}$
β_{zzz}^{e}	0.000	6.71×10^4
β_{zzz}^{nr}	0.000	8.01×10^3
η	0	0.12

$[Rb_3Be]^{2+}[B_6]^{6-}[Be'Rb'_3]^{4+}$. For D_{3d} $[Rb_3Be]^{3+}[B_6]^{6-}[Be'Rb'_3]^{3+}$, it is zero for both β_{zzz}^{e} and β_{zzz}^{nr}. So, there is a high-performance NLO switchable effect between $[Rb_3Be]^{2+}[B_6]^{6-}[Be'Rb'_3]^{4+}$ and $[Rb_3Be]^{3+}[B_6]^{6-}[Be'Rb'_3]^{3+}$ for both electronic and vibrational contributions.

Many experimental NLO investigations were performed by using the Z-scan method with laser pulses at wavelengths of 1064, 1340, 1560, and 1907 nm. Then, a frequency-dependent hyperpolarizability analysis has been carried out to the frequency-dependent fields (λ = ∝, 1064, 1340, 1560, and 1907 nm). Table 5 lists the TD-M06-2X and estimated MP2 $\beta_0(-2\omega,\omega,\omega)$, $\beta_{zzz}(-2\omega,\omega,\omega)$, and $\beta_{yyy}(-2\omega,\omega,\omega)$ values. The data in Table 5 show that it is pronounced for the differences between MP2 and the corresponding TD-M06-2X values for $\beta_0(-2\omega,\omega,\omega)$ of $[Rb_3Be]^{2+}[B_6]^{6-}[Be'Rb'_3]^{4+}$. Then, the TD-M06-2X values are used for the next discussion.

Owning to the D_{3d} point group, the frequency-dependent hyperpolarizability is zero for $[Rb_3Be]^{3+}[B_6]^{6-}[Be'Rb'_3]^{3+}$. The $\beta_0(-2\omega,\omega,\omega)$ values range from 1.42×10^5 to 3.15×10^8 au at above wavelengths. So, the frequency-dependent hyperpolarizability of $Rb_3BeB_6Be'Rb'_3$ also exhibits well-performance NLO switching effect from $[Rb_3Be]^{3+}[B_6]^{6-}[Be'Rb'_3]^{3+}$ (off form) to $[Rb_3Be]^{3+}[B_6]^{6-}[Be'Rb'_3]^{4+}$ (on form). It should be stressed that the contribution to $BeB_6Be'Rb'_3$ exhibits a good performance NLO switching effect from $[Rb_3Be]^{3+}[B_6]^{6-}[Be'Rb'_3]^{3+}$ (off form) to $[Rb_3Be]^{3+}[B_6]^{6-}[Be'Rb'_3]^{4+}$ (on-form). It should be stressed that the contribution to $\beta_0(-2\omega,\omega,\omega)$ is significantly different between $\beta_{zzz}(-2\omega,\omega,\omega)$ and $\beta_{yyy}(-2\omega,\omega,\omega)$ among different wavelengths of laser pulses. It is $\beta_{zzz}(-2\omega,\omega,\omega)$ at λ = ∝ and 1906 nm, but it is $\beta_{yyy}(-2\omega,\omega,\omega)$ at λ = 1460, 1340, and 1064

Table 5. TD-M06-2X and Estimated MP2 Values of Frequency-Dependent Hyperpolarizabilities ($\beta_0(-2\omega,\omega,\omega)$, $\beta_{zzz}(-2\omega,\omega,\omega)$, and $\beta_{yyy}(-2\omega,\omega,\omega)$, in au) for $[Rb_3Be]^{3+}[B_6]^{6-}[Be'Rb'_3]^{3+}$ (1) and $[Rb_3Be]^{2+}[B_6]^{6-}[Be'Rb'_3]^{4+}$ (2)

	λ (nm)				
	∝	1906	1460	1340	1064
$\beta_0(-2\omega,\omega,\omega)$[a]					
1	0 (0)	0 (0)	0 (0)	0 (0)	0 (0)
2	1.42×10^5 (2.18×10^5)	1.78×10^5 (2.73×10^5)	4.87×10^6 (7.48×10^6)	3.15×10^8 (4.83×10^8)	9.67×10^5 (1.49×10^6)
$\beta_{zzz}(-2\omega,\omega,\omega)$[a]					
1	0 (0)	0 (0)	0 (0)	0 (0)	0 (0)
2	1.61×10^5 (3.52×10^5)	1.13×10^6 (2.48×10^6)	-3.45×10^5 (-7.53×10^5)	-1.32×10^5 (-2.89×10^5)	1.71×10^4 (3.73×10^4)
$\beta_{yyy}(-2\omega,\omega,\omega)$[a]					
1	0 (0)	0 (0)	0 (0)	0 (0)	0 (0)
2	5.04×10^4 (6.93×10^3)	3.32×10^5 (4.59×10^4)	3.32×10^6 (4.58×10^5)	-3.92×10^7 (-5.41×10^6)	1.13×10^6 (1.56×10^5)

[a]The MP2 values are within parentheses.

https://doi.org/10.1021/acsomega.3c04248
ACS Omega 2023, 8, 30612−30620

nm, which provides the larger contribution to the $\beta_0(-2\omega,\omega,\omega)$ value.

CONCLUSIONS

In summary, we have presented the results of a novel IMSR NLO switch, a boron-based sandwich-like complex $Rb_3BeB_6Be'Rb'_3$. An OEEF of $F_z \geq 50 \times 10^{-4}$ au can drive an excess electron to transfer from tetrahedral $Be'Rb'_3$ to Rb_3Be, and subsequently, the self-redox reaction occurs, and $[Rb_3Be]^{3+}[B_6]^{6-}[Be'Rb'_3]^{3+}$ (D_{3d}) changes to $[Rb_3Be]^{2+}[B_6]^{6-}[Be'Rb'_3]^{4+}$ (C_{3v}).

$[Rb_3Be]^{3+}[B_6]^{6-}[Be'Rb'_3]^{3+}$ (off-form) has zero μ_0 and β_0^e due to the D_{3d} symmetry. However, C_{3v} $[Rb_3Be]^{2+}[B_6]^{6-}[Be'Rb'_3]^{4+}$ (on-form) exhibits high-performance NLO responses. The latter has an μ_0 of 3.36 D and a β_0^e of 2.18×10^5 au. Both electronic and vibrational contributions exhibit good performance NLO switching effects from [Rb3Be]3+[B6]6−[Be′Rb′3]3+ (off form) to [Rb3Be]-3+[B6]6−[Be′Rb′3]4+ (on-form). The difference in the dynamic first hyperpolarizabilities between $[Rb_3Be]^{3+}[B_6]^{6-}[Be'Rb'_3]^{3+}$ and $[Rb_3Be]^{2+}[B_6]^{6-}[Be'Rb'_3]^{4+}$ is also pronounced. Therefore, $Rb_3BeB_6Be'Rb'_3$ may be a high-performance candidate for an IMSR NLO molecular switch because there exists significant contrast in NLO property between $[Rb_3Be]^{3+}[B_6]^{6-}[Be'Rb'_3]^{3+}$ and $[Rb_3Be]^{2+}[B_6]^{6-}[Be'Rb'_3]^{4+}$ and the OEEF of $F_z \geq 50 \times 10^{-4}$ au can trigger from the former to change into the later.

ASSOCIATED CONTENT

Supporting Information

The Supporting Information is available free of charge at https://pubs.acs.org/doi/10.1021/acsomega.3c04248.

Data of optimized geometries, stability analysis, and the first hyperpolarizabilities (PDF)

AUTHOR INFORMATION

Corresponding Authors

Yin-Feng Wang − *Jiangxi Province Key Laboratory of Coordination Chemistry, Institute of Applied Chemistry, School of Chemistry and Chemical Engineering, Jinggangshan University, Ji'an CN 343009, China*; orcid.org/0000-0002-4597-7136; Email: cyclont@yeah.net

Zhi-Ru Li − *Laboratory of Theoretical and Computational Chemistry, Institute of Theoretical Chemistry, Jilin University, Changchun CN 130023, China*; orcid.org/0000-0002-1384-0725; Email: lzr@jlu.edu.cn

Authors

Jia-Mei Zeng − *Jiangxi Province Key Laboratory of Coordination Chemistry, Institute of Applied Chemistry, School of Chemistry and Chemical Engineering, Jinggangshan University, Ji'an CN 343009, China*

Qin Liu − *Jiangxi Province Key Laboratory of Coordination Chemistry, Institute of Applied Chemistry, School of Chemistry and Chemical Engineering, Jinggangshan University, Ji'an CN 343009, China*

Jing-Yi Zhao − *Jiangxi Province Key Laboratory of Coordination Chemistry, Institute of Applied Chemistry, School of Chemistry and Chemical Engineering, Jinggangshan University, Ji'an CN 343009, China*

Rui Deng − *Jiangxi Province Key Laboratory of Coordination Chemistry, Institute of Applied Chemistry, School of Chemistry and Chemical Engineering, Jinggangshan University, Ji'an CN 343009, China*

Jiangen Huang − *Jiangxi Province Key Laboratory of Coordination Chemistry, Institute of Applied Chemistry, School of Chemistry and Chemical Engineering, Jinggangshan University, Ji'an CN 343009, China*

Complete contact information is available at: https://pubs.acs.org/10.1021/acsomega.3c04248

Notes

The authors declare no competing financial interest.

ACKNOWLEDGMENTS

This work was supported by the National Natural Science Foundation of China (No. 21662018 and 21965015) and the Science and Technology Project of Jiangxi Provincial Department of Education (No. GJJ211016).

REFERENCES

(1) Ciampi, S.; Darwish, N.; Aitken, H. M.; Diez-Pérez, I.; Coote, M. L. Harnessing Electrostatic Catalysis in Single Molecule, Electrochemical and Chemical Systems: A Rapidly Growing Experimental Toolbox. *Chem. Soc. Rev.* **2018**, *47*, 5146−5164.

(2) Shaik, S.; Ramanan, R.; Danovich, D.; Mandal, D. Structure and reactivity/selectivity control by oriented-external electric fields. *Chem. Soc. Rev.* **2018**, *47*, 5125−5145.

(3) Stuyver, T.; Danovich, D.; Joy, J.; Shaik, S. External electric field effects on chemical structure and reactivity. *Wiley Interdiscip. Rev.: Comput. Mol. Sci.* **2020**, *10*, No. e1438.

(4) Fried, S. D.; Boxer, S. G. Electric Fields and Enzyme Catalysis. *Annu. Rev. Biochem.* **2017**, *86*, 387−415.

(5) Warshel, A.; Sharma, P. K.; Kato, M.; Xiang, Y.; Liu, H.; Olsson, M. H. M. Electrostatic Basis for Enzyme Catalysis. *Chem. Rev.* **2006**, *106*, 3210−3235.

(6) Finkelmann, A. R.; Stiebritz, M. T.; Reiher, M. Electric-field Effects on the [FeFe]-Hydrogenase Active Site. *Chem. Commun.* **2013**, *49*, 8099−8101.

(7) Aragonés, A. C.; Haworth, N. L.; Darwish, N.; Ciampi, S.; Bloomfield, N. J.; Wallace, G. G.; Diez-Perez, I.; Coote, M. L. Electrostatic catalysis of A Diels−Alder reaction. *Nature* **2016**, *531*, 88−91.

(8) Wang, Z.; Danovich, D.; Ramanan, R.; Shaik, S. Oriented-External Electric Fields Create Absolute Enantioselectivity in Diels−Alder Reactions: Importance of the Molecular Dipole Moment. *J. Am. Chem. Soc.* **2018**, *140*, 13350−13359.

(9) Aitken, H. M.; Coote, M. L. Can Electrostatic Catalysis of Diels−Alder Reactions Be Harnessed with Ph-Switchable Charged Functional Groups? *Phys. Chem. Chem. Phys.* **2018**, *20*, 10671−10676.

(10) Shaik, S.; Mandal, D.; Ramanan, R. Oriented electric fields as future smart reagents in chemistry. *Nat. Chem.* **2016**, *8*, 1091−1098.

(11) Zhou, Z.-J.; Li, X.-P.; Liu, Z.-B.; Li, Z.-R.; Huang, X.-R.; Sun, C.-C. Electric Field-Driven Acid-Base Chemistry: Proton Transfer from Acid (HCl) to Base (NH_3/H_2O). *J. Phys. Chem. A* **2011**, *115*, 1418−1422.

(12) Bai, Y.; He, H.-M.; Li, Y.; Li, Z.-R.; Zhou, Z.-J.; Wang, J.-J.; Wu, D.; Chen, W.; Gu, F.-L.; Sumpter, B. G.; Huang, J. Electric Field Effects on the Intermolecular Interactions in Water Whiskers: Insight from Structures, Energetics, and Properties. *J. Phys. Chem. A* **2015**, *119*, 2083−2090.

(13) Champagne, B.; Plaquet, A.; Pozzo, J.; Rodriguez, V.; Castet, F. Nonlinear Optical Molecular Switches as Selective Cation Sensors. *J. Am. Chem. Soc.* **2012**, *134*, 8101−8103.

(14) Zhai, Y.; Xu, W.; Meng, X.; Hou, H. Adjusting the Third-Order Nonlinear Optical Switch Performance Based on Azobenzene Derivatives. *Acta Chim. Sinica* **2020**, *78*, 256−262.

(15) Avramopoulos, A.; Zaleśny, R.; Reis, H.; Papadopoulos, M. G. A Computational Strategy for The Design of Photochromic

Derivatives Based on Diarylethene and Nickel Dithiolene with Large Contrast in Nonlinear Optical Properties. *J. Phys. Chem. C* **2020**, *124*, 4221−4241.
(16) Zhang, S.-Y.; Shu, X.; Zeng, Y.; Liu, Q.-Y.; Du, Z.-Y.; He, C.-T.; Zhang, W.-X.; Chen, X.-M. Molecule-Based Nonlinear Optical Switch with Highly Tunable On-Off Temperature Using a Dualsolid Solution Approach. *Nat. Commun.* **2020**, *11*, No. 2752.
(17) Beaujean, P.; Champagne, B. Unraveling the Symmetry Effects on The Second-Order Nonlinear Optical Responses of Molecular Switches: The Case of Ruthenium Complexes. *Inorg. Chem.* **2022**, *61*, 1928−1940.
(18) Xiang, Y.; Liang, G.; Alvaro, P.; Hu, X.; Liang, Y.; Kelly, T.-S.; Shi, Z.; Xu, H.; Chen, Z. Resonant Optical Nonlinearity and Fluorescence Enhancement in Electrically Tuned Plasmonic Nanosuspensions. *Adv. Photonics Res.* **2021**, *2*, No. 2000046.
(19) Liu, Z.; Wang, X.; Lu, T.; Yuan, A.; Yan, X. Potential Optical Molecular Switch: Lithium@Cyclo[18]Carbon Complex Transforming Between Two Stable Configurations. *Carbon* **2022**, *187*, 78−85.
(20) He, H.-M.; Li, Y.; Yang, H.; Yu, D.; Li, S.-Y.; Wu, D.; Hou, J.-H.; Zhong, R.-L.; Zhou, Z.-J.; Gu, F.-L.; Luis, J. M.; Li, Z.-R. Efficient External Electric Field Manipulated Nonlinear Optical Switches of All-Metal Electride Molecules with Infrared Transparency: Nonbonding Electron Transfer Forms an Excess Electron Lone Pair. *J. Phys. Chem. C* **2017**, *121*, 958−968.
(21) Wang, Y.-F.; Li, J.; Huang, J.; Qin, T.; Liu, Y.-M.; Zhong, F.; Zhang, W.; Li, Z.-R. Long-Range Charge Transfer Driven by External Electric Field in Alkalides M-LCaL-M (M = Li or Na, L = All-cis 1,2,3,4,5,6-Hexafluorocyclohexane): Facially Polarized Janus-Type Second Order Nonlinear Molecular Optical Switches. *J. Phys. Chem. C* **2019**, *123*, 23610−23619.
(22) Li, B.; Peng, D.; Gu, F.-L.; Zhu, C. A Nonlinear Optical Switch Induced by an External Electric Field: Inorganic Alkaline-Earth Alkalide. *RSC. Adv.* **2019**, *9*, 16718−16728.
(23) Hou, J.; Liu, Y.; Zhang, X.; Duan, Q.; Jiang, D.; Qin, J.; Zhao, R. Electric-Field-Induced Nonlinear Optical Switches of All-Metal Spherical Aromatic Molecules with Infrared Transparency: A Theoretical Study. *New. J. Chem.* **2018**, *42*, 1031−1036.
(24) Wang, Z.-J.; Wang, Y.-F.; Zeng, J.-M.; Zhang, W.; Liu, X.-X.; Li, J.; Li, Z.-R. Theoretical Insights into Single-Pole Quadruple-Throw (SP4T) Inorganic Nonlinear Optics Molecular Switch of Na-$(HCN)_3$Na: From Superalkali to Superalkalides. *J. Mater. Chem. C* **2022**, *10*, 16789−16802.
(25) Wang, Y.-F.; Qin, T.; Wang, J.-J.; Liu, X.-X.; Wang, Z.-J.; Huang, J.; Li, J.; Li, Z.-R. Switching from an Electride-Like Molecule to The Molecular Electride K-$F_6C_6H_6$ Driven by an Oriented External Electric Field. *Phys. Chem. Chem. Phys.* **2021**, *23*, 1443−1453.
(26) Wang, Y.-F.; Wang, J.-J.; Li, J.; Liu, X.-X.; Wang, Z.-J.; Huang, J.; Li, Z.-R. From an Electride-Like Super Alkali Earth Atom to a Superalkalide or Superalkali Electride: $M(HF)_3M$ (M = Na or Li) as Field-Induced Excellent Inorganic NLO Molecular Switches. *J. Mater. Chem. C* **2021**, *9*, 14885−14896.
(27) Yi, X.-G.; Wang, Y.-F.; Qin, T.; Liu, X.-X.; Jiang, S.-L.; Huang, J.; Yang, K.; Li, J.; Li, Z.-R. Electric Field Induced Intra-Molecular Self-Redox: Superalkali Li_3N_3Mg as a Candidate for NLO Molecular Switches. *Phys. Chem. Chem. Phys.* **2020**, *22*, 21928−21937, DOI: 10.1039/D0CP03113E.
(28) Zhang, F.-Y.; Xu, H.-L.; Su, Z.-M. Redox-Switchable Structures and NLO Property: Li2 Doped into The Cavity of Pyridine Helix. *Org. Electron.* **2018**, *57*, 68−73.
(29) Li, X.; Wang, H.-Q.; Ye, J.-T.; Zhang, Y.; Qiu, Y.-Q. Second-Order NLO Properties of Bis-Cyclometalated Iridium(III) Complexes: Substituent Effect and Redox Switch. *J. Mol. Graphics Modell.* **2019**, *89*, 131−138.
(30) Wang, Y.-J.; Feng, L.-Y.; Xu, L.; Hou, X.-R.; Li, N.; Miao, C.-Q.; Zhai, H.-J. Boron-Based Ternary $Rb_6Be_2B_6$ Cluster Featuring Unique Sandwich Geometry and a Naked Hexagonal Boron Ring. *Phys. Chem. Chem. Phys.* **2020**, *22*, 20043−20049.
(31) Frisch, M. J.; Trucks, G. W.; Schlegel, H. B.; Scuseria, G. E.; Robb, M. A.; Cheeseman, J. R.; Scalmani, G.; Barone, V.; Mennucci, B.; Petersson, G. A.et al. *Gaussian 09*, Revision A.02; Gaussian, Inc.: Wallingford CT, 2009.
(32) Adamo, C.; Barone, V. Toward Reliable Density Functional Methods Without Adjustable Parameters: The PEB0Model. *J. Chem. Phys.* **1999**, *110*, 6158−6170.
(33) Weigend, F.; Ahlrichs, R. Balanced Basis Sets Of Split Valence, Triple Zeta Valenceand Quadruple Zeta Valence Quality for H to Rn: Design And Assessment of Accuracy. *Phys. Chem. Chem. Phys.* **2005**, *7*, 3297−3305.
(34) Tian, Y.; Wei, D.; Jin, Y.; Barroso, J.; Lu, C.; Merino, G. Exhaustive exploration of MgB_n (n = 10 - 20) clusters and their anions. *Phys. Chem. Chem. Phys.* **2019**, *21*, 6935−6941.
(35) Lv, J.; Wang, Y.; Zhang, L.; Lin, H.; Zhao, J.; Ma, Y. Stabilization of Fullerene-Like Boron Cages By Transition Metal Encapsulation. *Nanoscale* **2015**, *7*, 10482−10489.
(36) Tian, W. Triple-ring Tubular MB_{36} (M = Mg, Ca, Sr, Ba) with Threefold Aromaticity. *Int. J. Quantum Chem.* **2021**, *121*, No. e26595.
(37) Dong, X.; Jalife, S.; Vásquez-Espinal, A.; Barroso, J.; Orozco-Ic, M.; Ravell, E.; Cabellos, J. L.; Liang, W.; Cui, Z.-h.; Merino, G. Li_2B_{24}: the Simplest Combination for a Three-ring Boron Tube. *Nanoscale* **2019**, *11*, 2143−2147.
(38) Glendening, E.; Badenhoop, J. K.; Reed, A. E.; Carpenter, J. E.; Bohmann, J. A.; Morales, C. M.; Weinhold, F. *NBO 3.0 Program*; University of Wisconsin: Madison, 2001.
(39) Bader, R. F. W. A Quantum Theory of Molecular Structure and Its Applications. *Chem. Rev.* **1991**, *91*, 893−928.
(40) Lu, T.; Chen, F. W. Multiwfn: A Multifunctional Wavefunction Analyser. *J. Comput. Chem.* **2012**, *33*, 580−592.
(41) Sowlati-Hashjin, S.; Matta, C. F. The Chemical Bond in External Electric Fields: Energies, Geometries, And Vibrational Stark Shifts of Diatomic Molecules. *J. Chem. Phys.* **2013**, *139*, No. 144101.
(42) Arabi, A. A.; Matta, C. F. Effects of Intense Electric Fields on the Double Proton Transfer in the Watson−Crick Guanine−Cytosine Base Pair. *J. Phys. Chem. B* **2018**, *122*, 8631−8641.
(43) Mohammed, A. A. K.; Limacher, P. A.; Champagne, B. Finding Optimal Finite Field Strengths Allowing for a Maximum of Precision in the Calculation of Polarizabilities and Hyperpolarizabilities. *J. Comput. Chem.* **2013**, *34*, 1497−1507.
(44) de Wergifosse, M.; Liégeois, V.; Champagne, B. Evaluation of the molecular static and dynamic first hyperpolarizabilities. *Int. J. Quantum Chem.* **2014**, *114*, 900−910.
(45) Yu, G.; Huang, X.-R.; Chen, W.; Sun, C.-C. Alkali Metal Atom-Aromatic Ring: A Novel Interactionmode Realizes Large First Hyperpolarizabilities of M@AR (M = Li, Na, And K, AR = Pyrrole, Indole, Thiophene, and Benzene). *J. Comput. Chem.* **2011**, *32*, 2006−2011.
(46) Gao, F. W.; Xu, H. L.; Su, Z. M. Tuning the Inter-Molecular Charge Transfer, Second-Order Nonlinear Optical and Absorption Spectra Properties of A π-Dimer Under an External Electric Field. *Phys. Chem. Chem. Phys.* **2017**, *19*, 31958−31964.
(47) Bishop, D. M.; Hasan, M.; Kirtman, B. A Simple Method for Determining Approximate Static and Dynamic Vibrational Hyperpolarizabilities. *J. Chem. Phys.* **1995**, *103*, 4157−4159.
(48) Dennington, R.; Keith, T. A.; Millam, J. M. *GaussView*, Version 6:Wallingford, CT, 2016.
(49) Wang, J.-J.; Zhou, Z.-J.; He, H.-M.; Wu, D.; Li, Y.; Li, Z.-R.; Zhang, H.-X. An External Electric Field Manipulated Second-Order Nonlinear Optical Switch of an Electride Molecule: A Long-Range Electron Transfer Forms a Lone Excess Electron Pair and Quenches Singlet Diradical. *J. Phys. Chem. C* **2016**, *120*, 13656−13666.
(50) Gruebele, M.; Zewail, A. H. Turbulence: Challenges for Theory and Experiment. *Phys. Today* **1990**, *43*, 24−35.
(51) Kanis, D. R.; Ratner, M. A.; Marks, T. J. Design and Construction of Molecular Assemblies with Large Second-Order Optical Nonlinearities. Quantum Chemical Aspects. *Chem. Rev.* **1994**, *94*, 195−242.

https://doi.org/10.1021/acsomega.3c04248
ACS Omega 2023, 8, 30612−30620